Supplementary Material to manuscript entitled *Investigating the spatial representativeness of Antarctic ice cores: A comparison of ice core and radar-derived surface mass balance*

Marie G.P. Cavitte[1], Hugues Goosse[1], Kenichi Matsuoka[2], Sarah Wauthy[3], Vikram Goel[4], Rahul Dey[4], Bhanu Pratap[4], Brice Van Liefferinge[5], Thamban Meloth[4], and Jean-Louis Tison[3]

[1]Earth and Life Institute (ELI), Université catholique de Louvain-La-Neuve (UCLouvain), Louvain-la-Neuve, Belgium
[2]Norwegian Polar Institute, Tromsø, Norway
[3]Laboratoire de Glaciologie, Université libre de Bruxelles (ULB), Brussels, Belgium
[4]National Centre for Polar and Ocean Research (NCPOR), Ministry of Earth Sciences, Vasco-da Gama, Goa 403804, India
[5]SPF Interieur, Brussels, Belgium

Correspondence: Marie Cavitte (marie.cavitte@uclouvain.be)

S1 Best-fit density profiles

We outline the best-fit depth-density profiles for each study site, density ρ is in g cm^{-3} and depth z is in meters. For the coastal ice rises, the best-fits are obtained applying the Hubbard et al. (2013) exponential depth-density fit, using a surface density that matches best that of the surface, and changing the other two parameters until the R^2 fit between the raw ice core densities and the fit is minimized, from the interval comprised between the surface and the depth of the deepest IRH of the radar survey. For Dome Fuji, we use the Van Liefferinge et al. (2021) linear relationship provided between depth and density.

- Blåskimen Island: $\rho = 0.910 - 0.4261\ e^{-0.024z}$ ($R^2 = 0.93$)
- Kupol Moskovskij: $\rho = 0.910 - 0.4599\ e^{-0.034z}$, ($R^2 = 0.96$)
- Kupol Ciolkovskogo: $\rho = 0.910 - 0.4735\ e^{-0.038z}$, ($R^2 = 0.95$)
- Djupranen: $\rho = 0.910 - 0.4835\ e^{-0.033z}$, ($R^2 = 0.85$)
- Leningradkollen: $\rho = 0.910 - 0.4846\ e^{-0.045z}$, ($R^2 = 0.64$)
- Hammarryggen: $\rho = 0.910 - 0.465\ e{-}0.028z$, ($R^2 = 0.99$)
- Lokkeryggen: $\rho = 0.910 - 0.450\ e^{-0.030z}$, ($R^2 = 0.99$)
- Derwael: $\rho = 0.910 - 0.510\ e^{-0.026z}$, ($R^2 == 0.98$)
- Dome Fuji: $\rho = 0.00911\ z + 0.331$, ($R^2 = 0.39$)

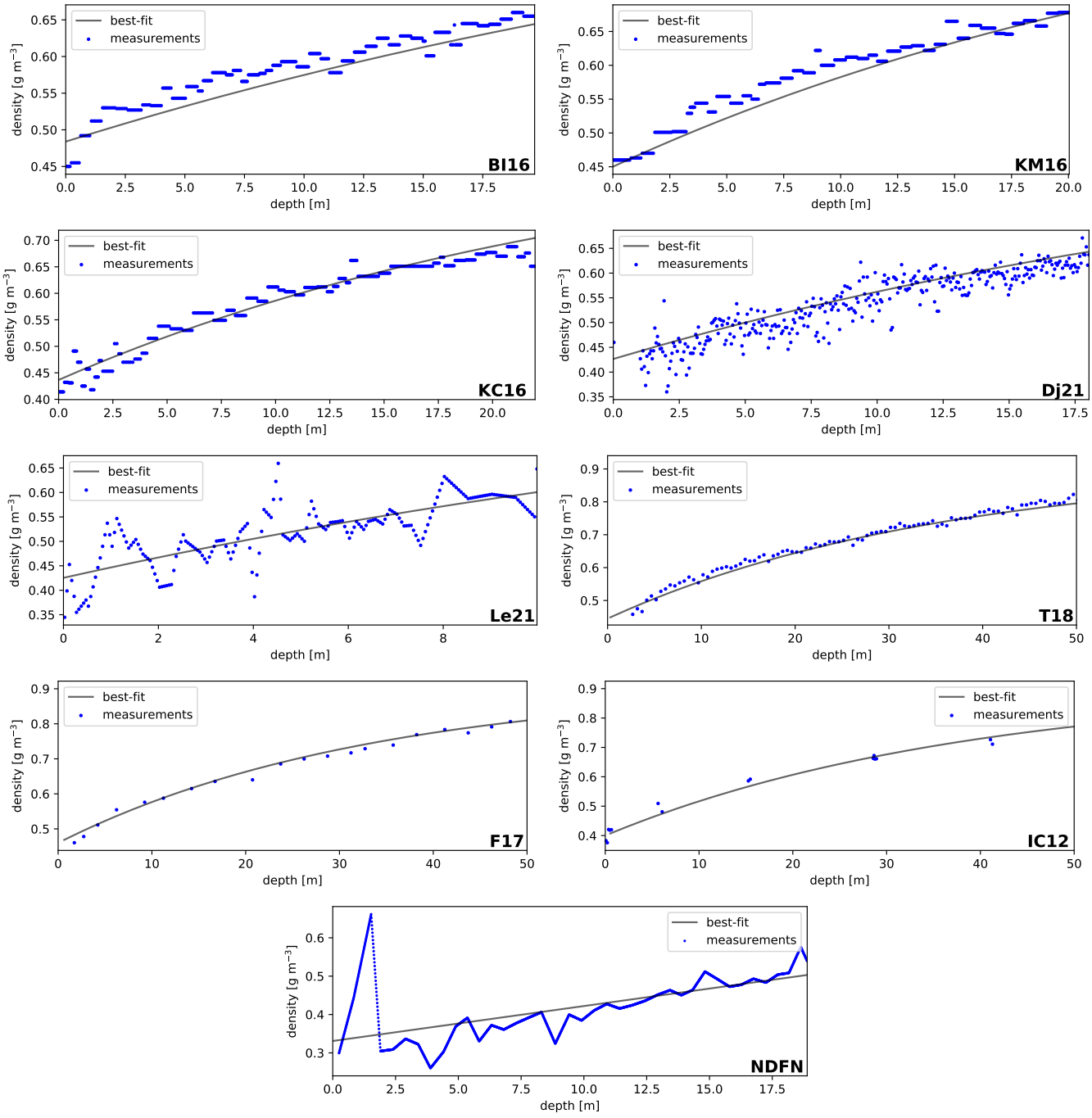

Figure S1. Density profiles for each ice core. Raw density measurements in blue and best-fit exponential or linear profile in black.

Fig. S1 shows the raw ice core densities and the best-fit profiles from the surface to teh deepest IRH traced at each site.

The best-fit density profiles can then be integrated as a function of depth, to obtain a profile of cumulative mass versus depth. Cumulative mass CM_k (expressed in m w.e.) from the surface and a given depth z is given by the expressions below:

- Blåskimen Island: $CM_k = 0.910\ z + \frac{0.4261}{0.024}\ e^{-0.024z} - 17.75$
- Kupol Moskovski: $CM_k = 0.910\ z + \frac{0.4599}{0.034}\ e^{-0.034z} - 13.53$
- Kupol Ciolkovskogo: $CM_k = 0.910\ z + \frac{0.4735}{0.038}\ e^{-0.038z} - 12.46$
- Djupranen: $CM_k = 0.910\ z + \frac{0.4835}{0.033}\ e^{-0.033z} - 14.65$
- Leningradkollen: $CM_k = 0.910\ z + \frac{0.4846}{0.045}\ e^{-0.045z} - 10.77$
- Hammarryggen: $CM_k = 0.910\ z + \frac{0.465}{0.028}\ e{-0.028z} - 16.61$
- Lokkeryggen: $CM_k = 0.910\ z + \frac{0.450}{0.03}\ e^{-0.030z} - 15.00$
- Derwael: $CM_k = 0.910\ z + \frac{0.510}{0.026}\ e^{-0.026z} - 19.62$
- Dome Fuji: $CM_k = \frac{0.00911}{2} z^2 + 0.331\ z$

S2 Radar density spatial variability

We show the spatial variability of the density profiles calculated for every point of each radar survey. This is used to constrain the density-related SMB uncertainty.

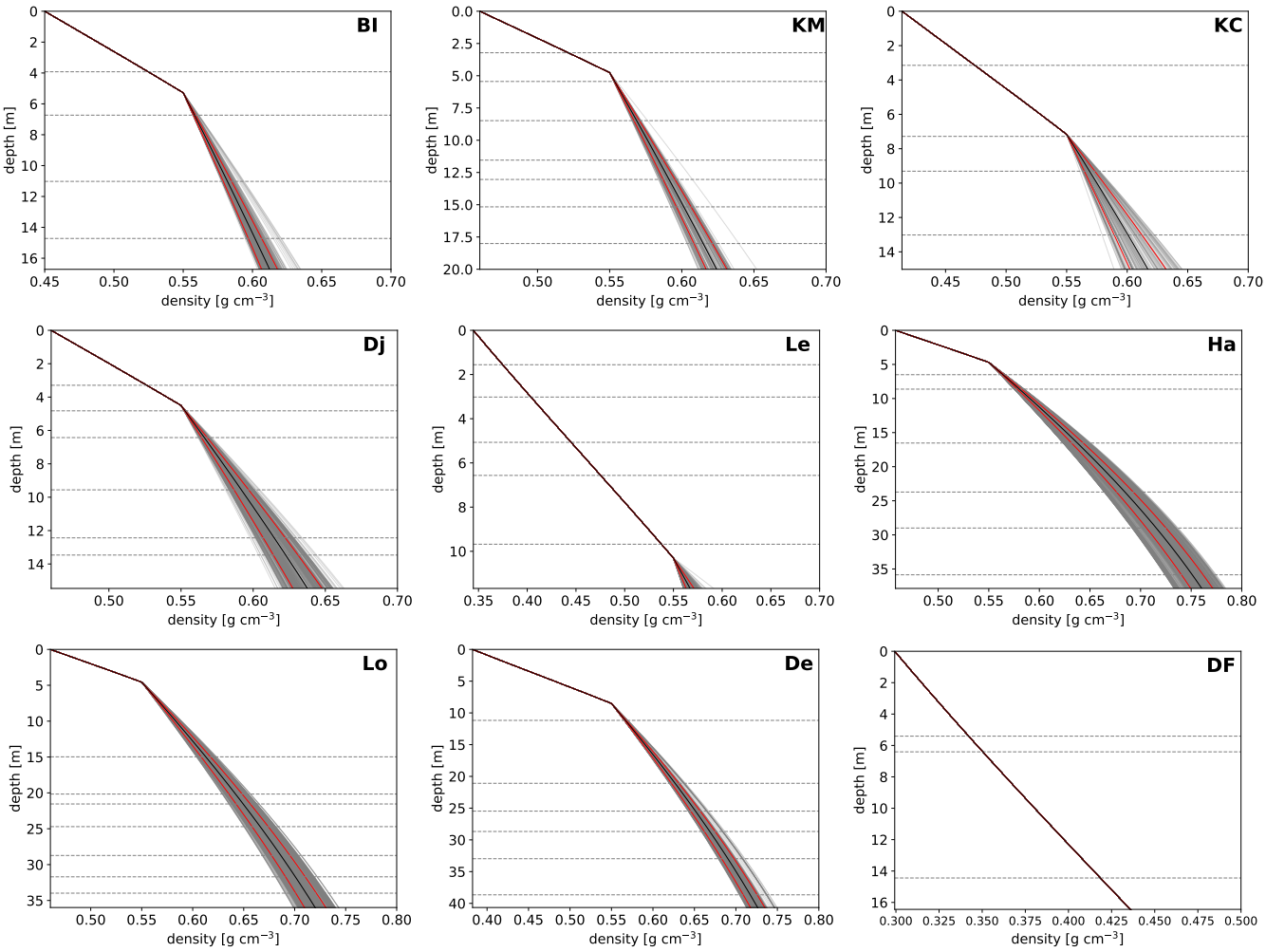

Figure S2. Spatial variability of the density, calculated for each radar data point. Each panel shows the result for a study site, with the site labeled in the top right corner. The black curve is the calculated mean density over the entire radar survey, the gray curves show each individual density profile and the red curves show the 1 standard deviation error. Horizontal black dashed lines highlight the radar IRH depths for context. Note that the vertical and the horizontal scales vary from site to site.

S3 SMB uncertainties for each site

We provide the calculated SMB uncertainty site by site, and as a function of depth, for the ice core and the radar data, in Tables S1 and S2.

Table S1. Radar SMB uncertainty for each site, given in % of the radar-derived SMB for each time interval.

Interval	BI	KM	KC	Dj	Le	Ha	Lo	De	DF
1	1.7	1.7	1.8	2.8	5.8	0.9	0.5	0.6	1.1
2	1.7	1.8	1.9	2.9	6.1	1.0	1.0	0.7	1.2
3	1.8	1.9	2.0	3.0	6.4	1.2	1.7	1.2	1.3
4	2.0	2.0	2.4	3.2	6.7	1.8	2.5	1.8	
5		2.1		3.4	6.9	2.6	3.4	2.5	
6		2.5		3.9		3.5	4.4	3.3	
7		3.0					5.4		

Table S2. Ice core SMB uncertainty for each site, given in % of the ice core SMB for each time interval.

Interval	BI	KM	KC	Dj	Le	Ha	Lo	De	NDFN
1	3.8	4.1	3.7	6.3	8.5	3.5	1.8	5.0	16.5
2	3.6	3.7	3.3	5.9	8.0	3.2	1.5	4.1	15.2
3	3.4	3.5	3.0	5.7	7.5	2.9	1.5	3.7	13.7
4	3.2	3.3	2.9	5.3	7.0	2.7	1.4	3.6	
5		3.2		5.0	6.6	2.5	1.4	3.5	
6		3.1		4.8		2.4	1.4	3.3	
7		3.0					1.3		

S4 SMB spatial distribution through time

We show the spatial distribution of SMB for each time interval for all sites, except BI already shown in Fig. 4 of the main manuscript.

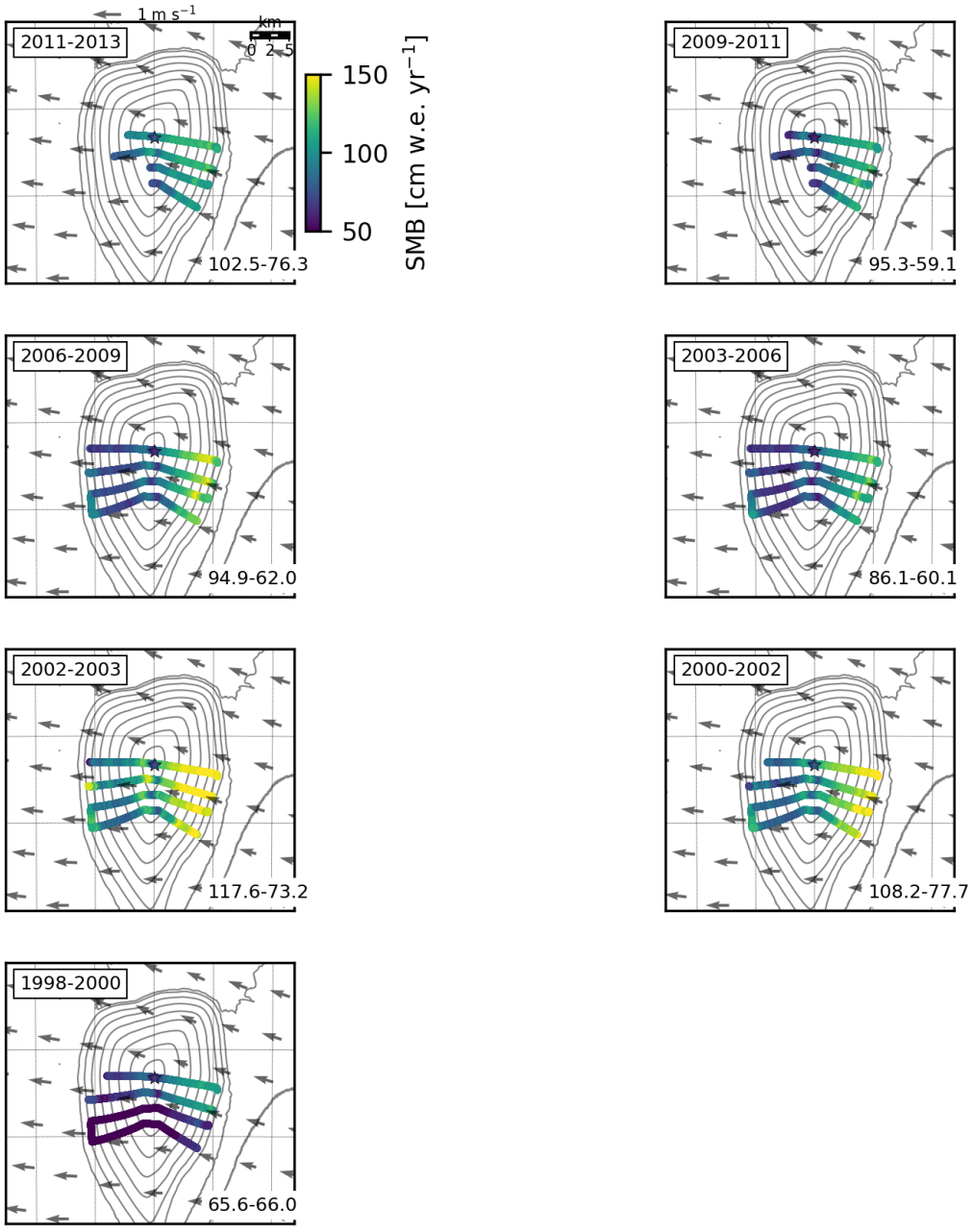

Figure S3. Spatial distribution of SMB through time at KM. Each panel represents a different time interval, going from most recent at the top left, to the oldest at the bottom right. Contours are REMA v2.0 elevation contours, with a 30 m interval, gray arrows show the mean wind direction (RACMO2.3 5.5 km simulations over 1979–2017, Lenaerts et al. (2017); Van Wessem et al. (2018)). The wind magnitude scale is shown on top of the first panel. Numbers in lower right corner of each panel are radar area average SMB – ice core SMB.

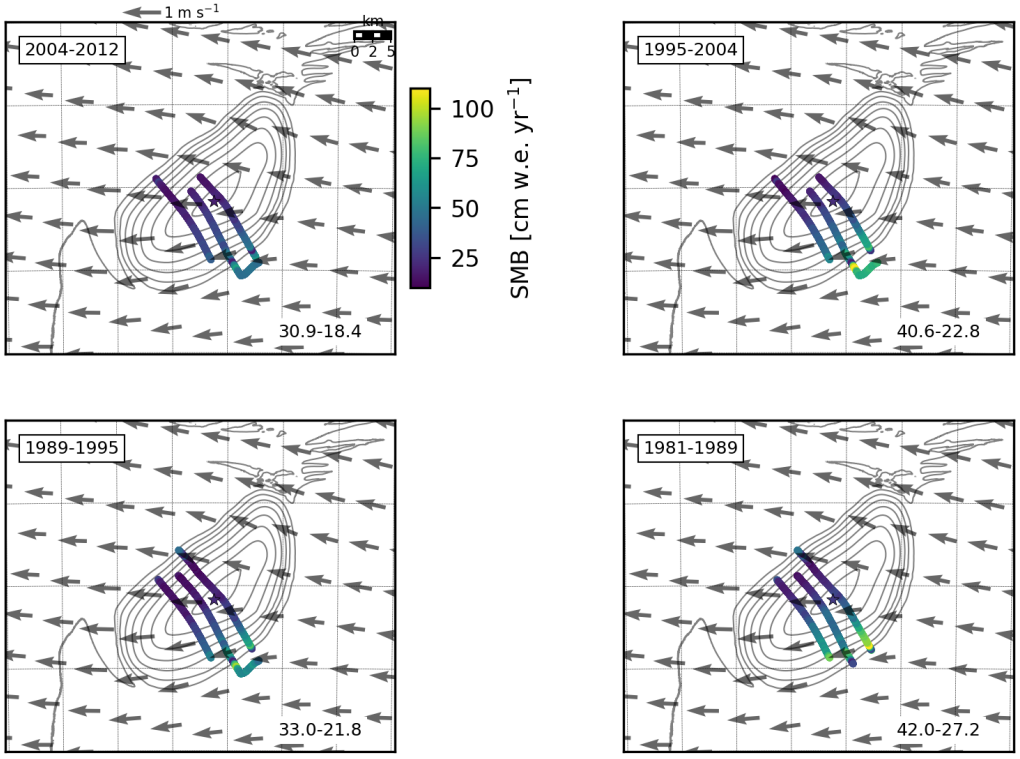

Figure S4. Spatial distribution of SMB through time at KC. Each panel represents a different time interval, going from most recent at the top left, to the oldest at the bottom right, the time intervals are provided in the top left corner of each frame. Contours are REMA v2.0 elevation contours, with a 30 m interval, gray arrows show the mean wind direction (RACMO2.3 5.5 km simulations over 1979–2017, Lenaerts et al. (2017); Van Wessem et al. (2018)). The wind magnitude scale is shown on top of the first panel. Numbers in lower right corner of each panel are radar area average SMB – ice core SMB in cm w.e. yr^{-1}.

S5 Definition of the SMB temporal variability

The uncertainty in measuring temporal variability from a point measurement Δobs_t is calculated as the amplitude of the difference between the ice core SMB and the area averaged SMB at each site, provided from the radar spatial average. The mean SMB bias between the two proxies is first removed by calculate the ice core and the radar-derived SMB anomalies (i.e. SMB record minus its temporal mean), at each radar location. Δobs_t is defined as below, in m w.e. yr^{-1}:

$$\Delta obs_t = \sigma(\nu_{radar} - \nu_{ic}) \tag{S1}$$

with ν is the SMB residual of the proxy (SMB record minus its temporal mean), σ is the standard deviation and ic stands for ice core. The SMB residual of each proxy is given by $\nu = SMB - \overline{SMB}$, where $\overline{SMB}$ is the temporal mean of the SMB.

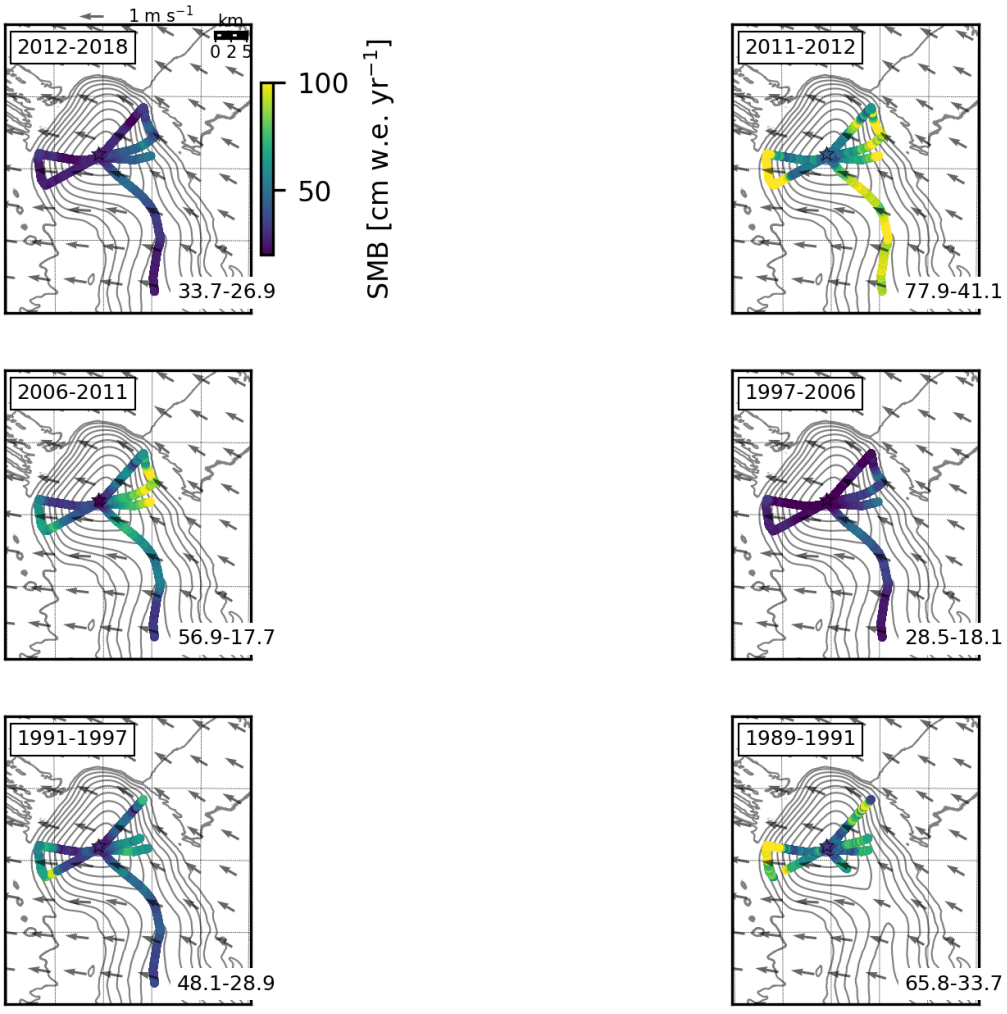

Figure S5. Spatial distribution of SMB through time at Dj. Each panel represents a different time interval, going from most recent at the top left, to the oldest at the bottom right, the time intervals are provided in the top left corner of each frame. Contours are REMA v2.0 elevation contours, with a 30 m interval, black arrows show the mean wind direction (RACMO2.3 5.5 km simulations over 1979–2017, Lenaerts et al. (2017); Van Wessem et al. (2018)). Numbers in lower right corner of each panel are radar area average SMB – ice core SMB in cm w.e. yr^{-1}.

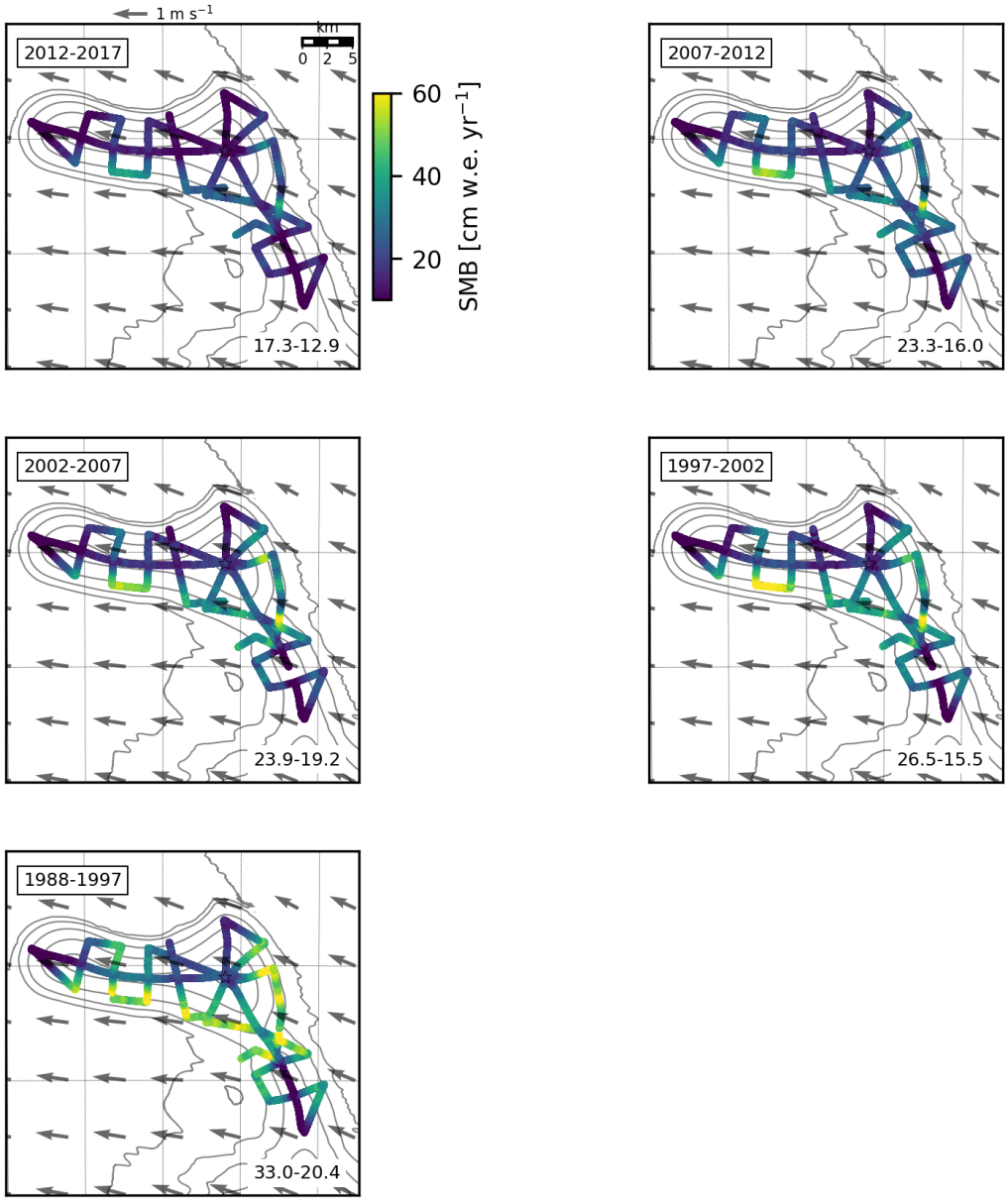

Figure S6. Spatial distribution of SMB through time at Le. Each panel represents a different time interval, going from most recent at the top left, to the oldest at the bottom right, the time intervals are provided in the top left corner of each frame. Contours are REMA v2.0 elevation contours, with a 30 m interval, gray arrows show the mean wind direction (RACMO2.3 5.5 km simulations over 1979–2017, Lenaerts et al. (2017); Van Wessem et al. (2018)). The wind magnitude scale is shown on top of the first panel. Numbers in lower right corner of each panel are radar area average SMB – ice core SMB in cm w.e. yr^{-1}.

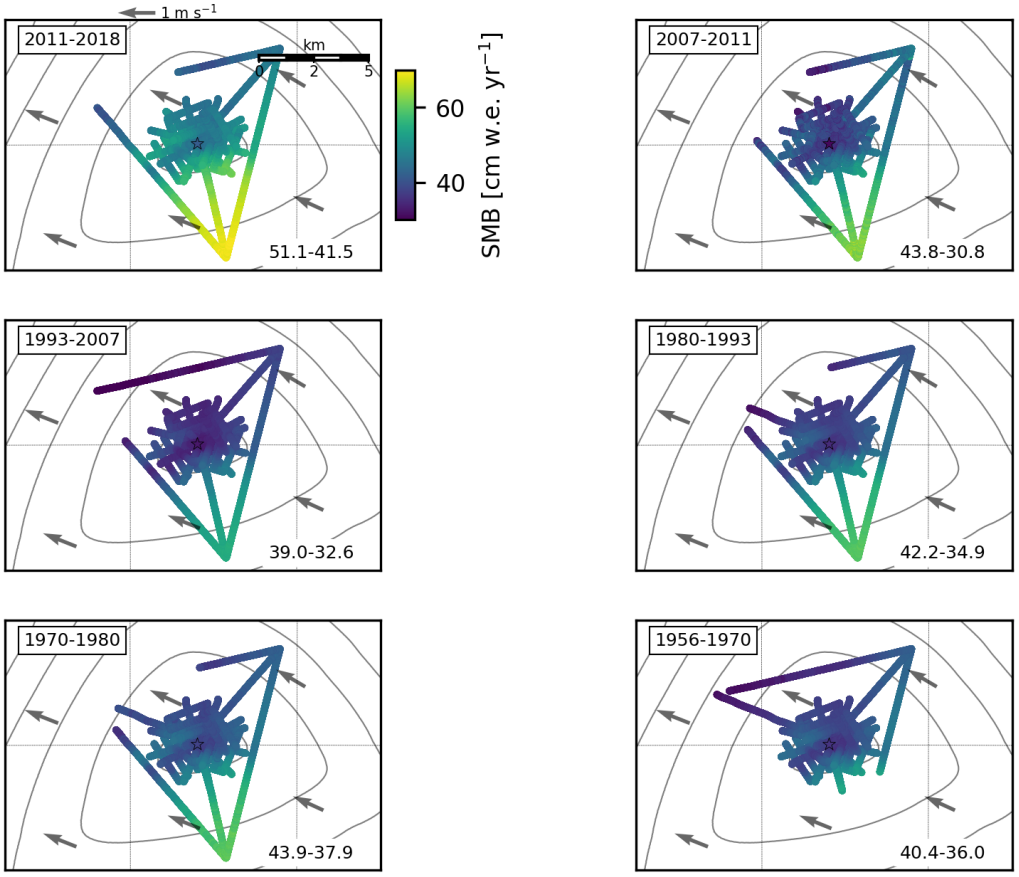

Figure S7. Spatial distribution of SMB through time at Ha. Each panel represents a different time interval, going from most recent at the top left, to the oldest at the bottom right, the time intervals are provided in the top left corner of each frame. Contours are REMA v2.0 elevation contours, with a 30 m interval, gray arrows show the mean wind direction (RACMO2.3 5.5 km simulations over 1979–2017, Lenaerts et al. (2017); Van Wessem et al. (2018)). The wind magnitude scale is shown on top of the first panel. Numbers in lower right corner of each panel are radar area average SMB – ice core SMB in cm w.e. yr^{-1}.

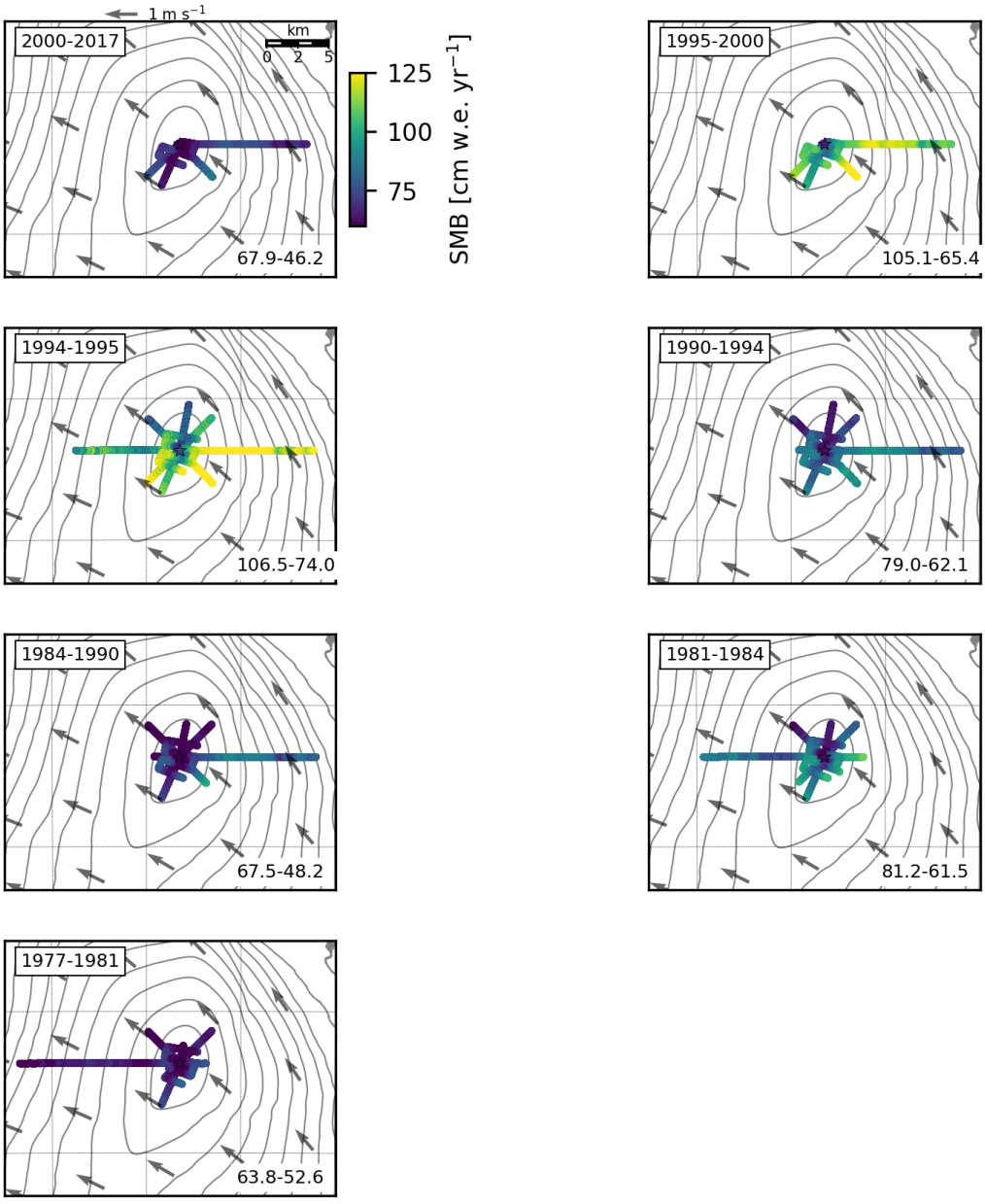

Figure S8. Spatial distribution of SMB through time at Lo. Each panel represents a different time interval, going from most recent at the top left, to the oldest at the bottom right, the time intervals are provided in the top left corner of each frame. Contours are REMA v2.0 elevation contours, with a 30 m interval, gray arrows show the mean wind direction (RACMO2.3 5.5 km simulations over 1979–2017, Lenaerts et al. (2017); Van Wessem et al. (2018)). The wind magnitude scale is shown on top of the first panel. Numbers in lower right corner of each panel are radar area average SMB – ice core SMB in cm w.e. yr^{-1}.

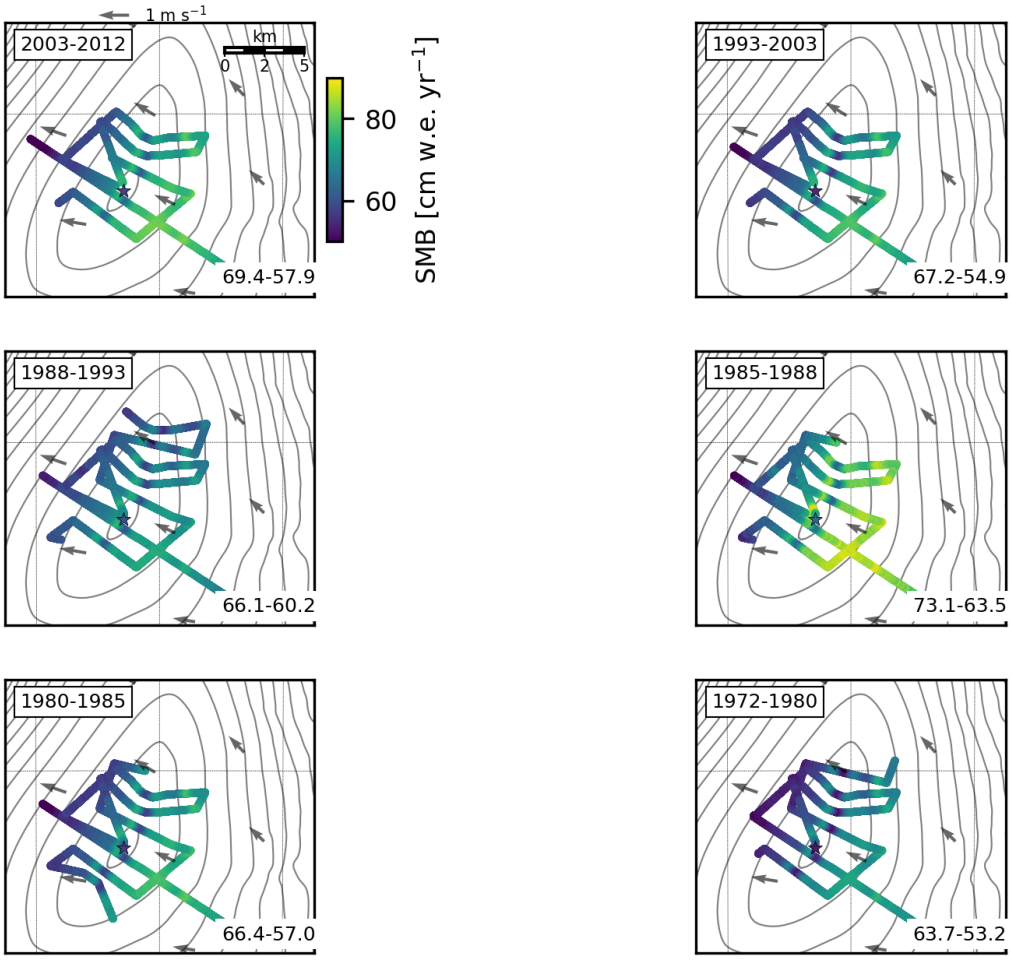

Figure S9. Spatial distribution of SMB through time at De. Each panel represents a different time interval, going from most recent at the top left, to the oldest at the bottom right, the time intervals are provided in the top left corner of each frame. Contours are REMA v2.0 elevation contours, with a 30 m interval, gray arrows show the mean wind direction (RACMO2.3 5.5 km simulations over 1979–2017, Lenaerts et al. (2017); Van Wessem et al. (2018)). The wind magnitude scale is shown on top of the first panel. Numbers in lower right corner of each panel are radar area average SMB – ice core SMB in cm w.e. yr^{-1}.

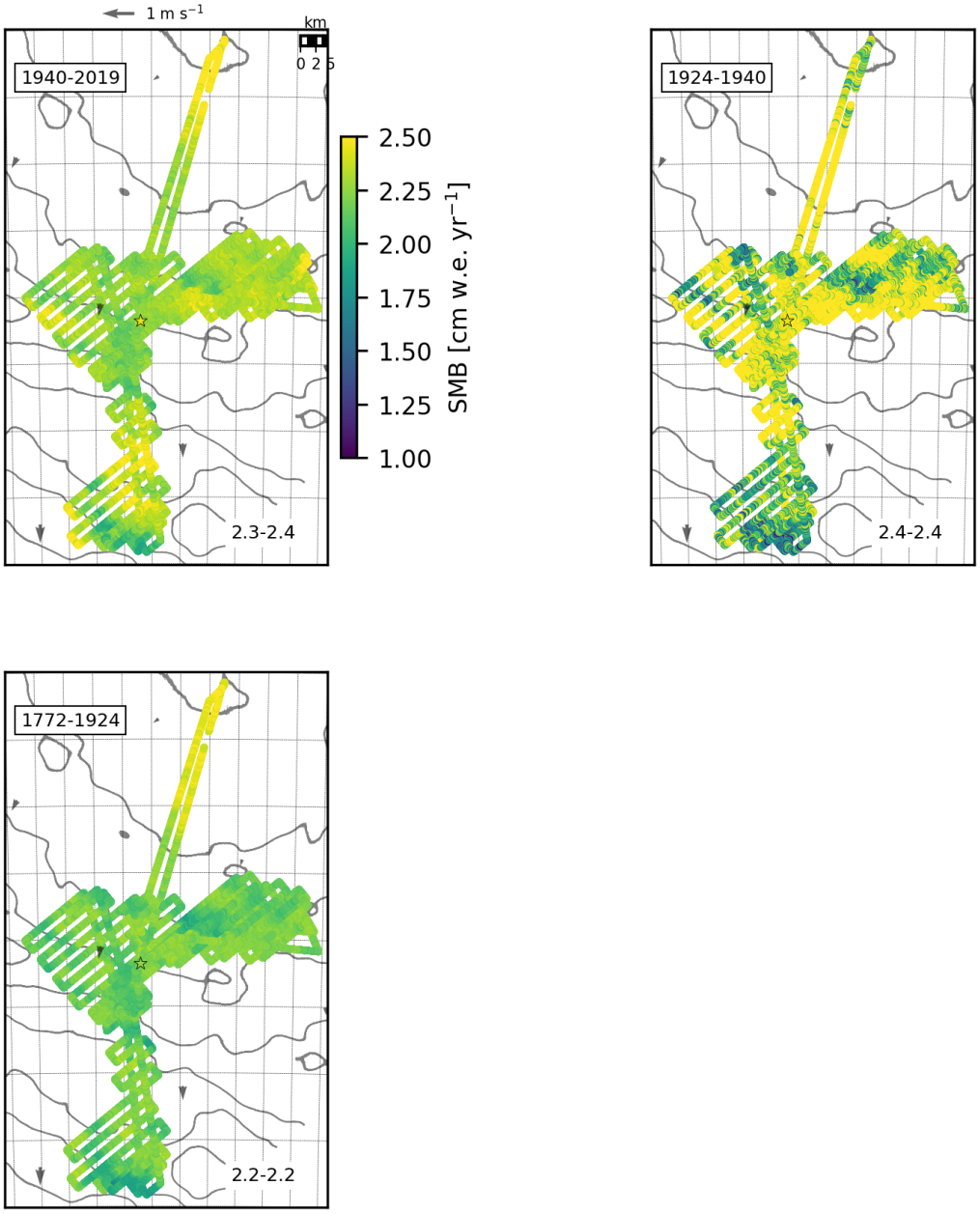

Figure S10. Spatial distribution of SMB through time at DF. Each panel represents a different time interval, going from most recent at the top left, to the oldest at the bottom right, the time intervals are provided in the top left corner of each frame. Contours are REMA v2.0 elevation contours, with a 30 m interval, gray arrows show the mean wind direction (RACMO2.3 27 km simulations over 1979–2017, Lenaerts et al. (2017); Van Wessem et al. (2018)). The wind magnitude scale is shown on top of the first panel. Numbers in lower right corner of each panel are radar area average SMB – ice core SMB in cm w.e. yr^{-1}.

To normalize across sites with differing SMB rates, we normalize by the temporal variability of the ice core measurement defined, i.e. Δobs_t is normalized to the standard deviation of the ice core SMB residual, as defined below:

$$\Delta obs_t(\%) = \frac{\sigma(\nu_{radar} - \nu_{ic})}{\sigma(\nu_{ic})} \times 100 \tag{S2}$$

$$\Delta \mu_t = \overline{SMB}_{radar} - \overline{SMB}_{ic} \tag{S3}$$

S6 Quantification of the SMB representativeness

We show the relative difference in mean SMB between the point measurement (ice core) and the area mean, as well as the relative uncertainty in measuring temporal variability from a point measurement $\Delta obs_t(\%)$, for all radar product resolutions considered (Fig. S11). It is clear that the resolution chosen does not influence the result .

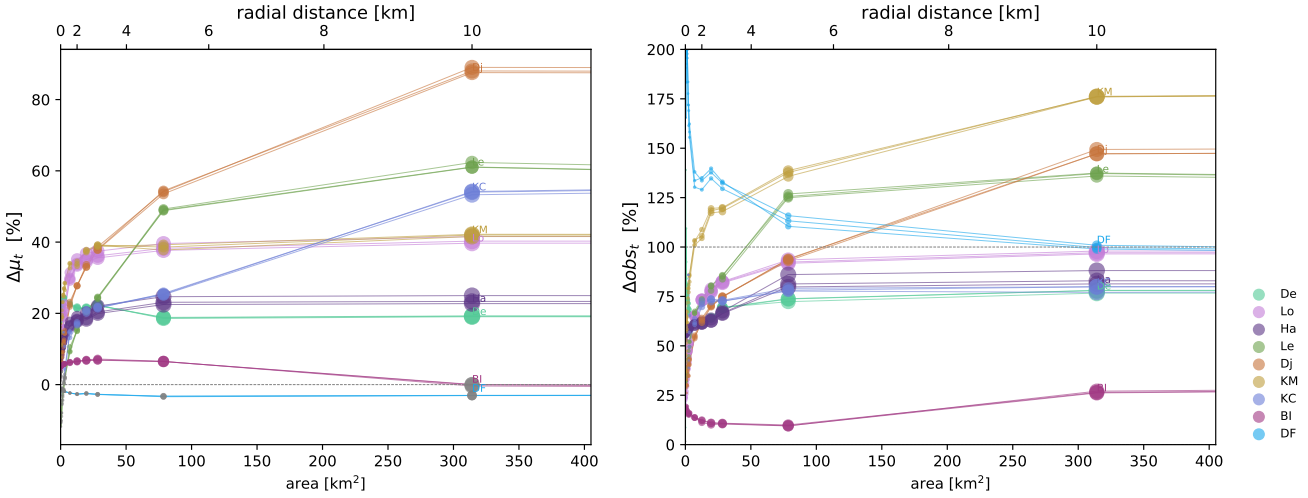

Figure S11. (left) Difference in mean SMB value between the point measurement (ice core) and the area mean and (right) the relative uncertainty in measuring temporal variability from a point measurement $\Delta obs_t(\%)$, for all radar product resolutions considered. Each site is represented by a different color, gray dots imply that the difference is negligible with respect to the SMB uncertainties. The size of the dots represents the number of grid points within the radial distance. The results obtained for all three radar gridding cell sizes are shown together (50 m, 100 m and 250 m square grid cells).

We also show the relative difference in mean SMB and the relative uncertainty in measuring temporal variability from a point measurement $\Delta obs_t(\%)$, as a function of (1) distance of the ice core from the grounding line, (2) mean SMB and (3) radar IRH average temporal resolution in Fig. S12.

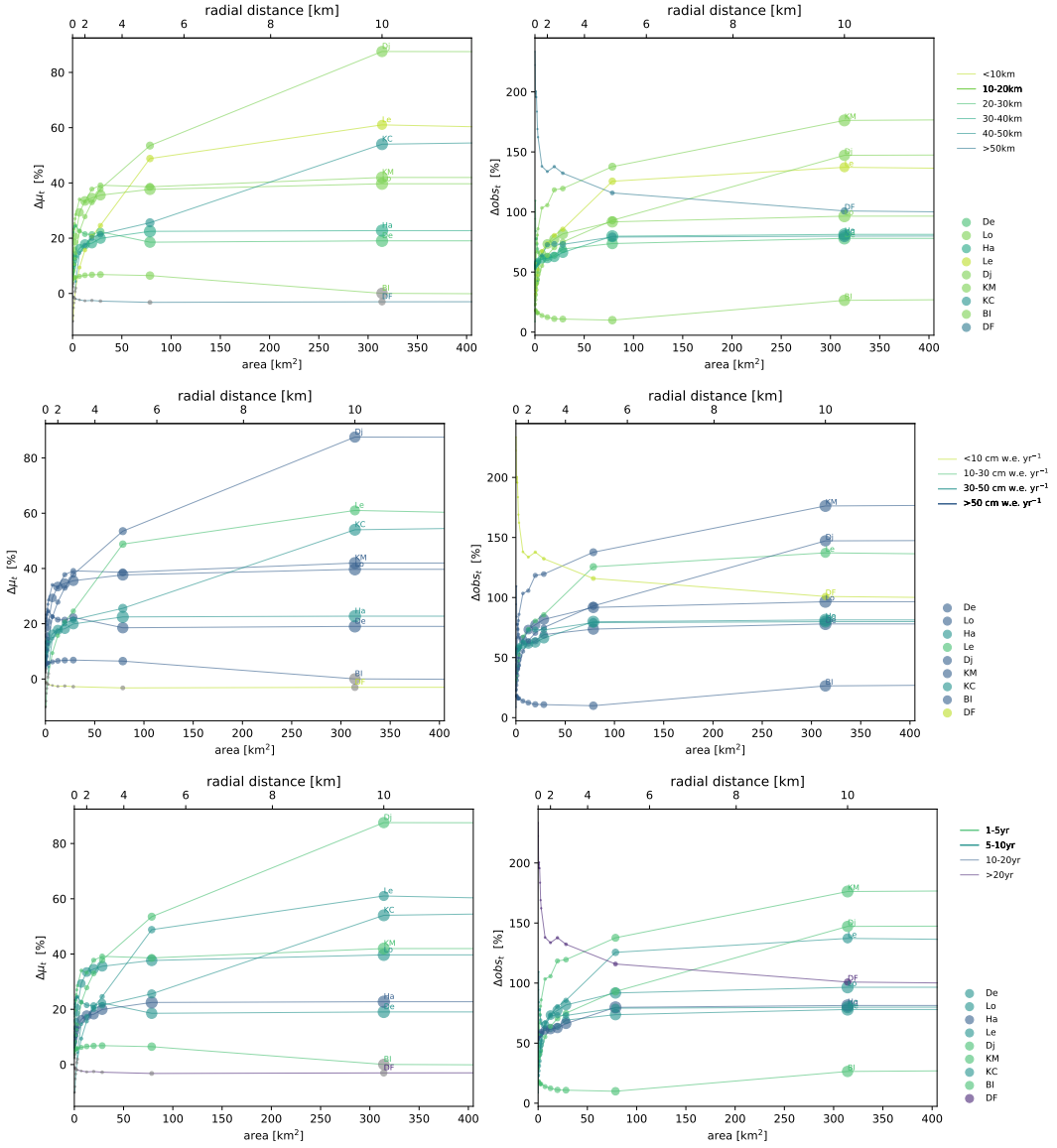

Figure S12. (left) Difference in mean SMB value between the point measurement (ice core) and the area mean (50 m gridded radar product resolution) and (right) the relative uncertainty in measuring temporal variability from a point measurement $\Delta obs_t(\%)$. Sites are colored by distance of the ice core from the grounding line (top), mean SMB (middle) and radar IRH average temporal resolution (bottom). Gray dots imply that the difference is negligible with respect to the SMB uncertainties. The size of the dots represents the number of grid points within the radial distance

References

Hubbard, B., Tison, J.-L., Philippe, M., Heene, B., Pattyn, F., Malone, T., and Freitag, J.: Ice shelf density reconstructed from optical televiewer borehole logging, Geophysical Research Letters, 40, 5882–5887, https://doi.org/10.1002/2013GL058023, 2013.

Lenaerts, J., Lhermitte, S., Drews, R., Ligtenberg, S., Berger, S., Helm, V., Smeets, C., Van den Broeke, M., Van De Berg, W. J., Van Meijgaard, E., et al.: Meltwater produced by wind–albedo interaction stored in an East Antarctic ice shelf, Nature climate change, 7, 58, 2017.

Van Liefferinge, B., Taylor, D., Tsutaki, S., Fujita, S., Gogineni, P., Kawamura, K., Matsuoka, K., Moholdt, G., Oyabu, I., Abe-Ouchi, A., Awasthi, A., Buizert, C., Gallet, J.-C., Isaksson, E., Motoyama, H., Nakazawa, F., Ohno, H., O'Neill, C., Pattyn, F., and Sugiura, K.: Surface Mass Balance Controlled by Local Surface Slope in Inland Antarctica: Implications for Ice-Sheet Mass Balance and Oldest Ice Delineation in Dome Fuji, Geophysical Research Letters, 48, e2021GL094 966, https://doi.org/10.1029/2021GL094966, e2021GL094966 2021GL094966, 2021.

Van Wessem, J. M., Jan Van De Berg, W., Noël, B. P., Van Meijgaard, E., Amory, C., Birnbaum, G., Jakobs, C. L., Krüger, K., Lenaerts, J., Lhermitte, S., et al.: Modelling the climate and surface mass balance of polar ice sheets using RACMO2: Part 2: Antarctica (1979-2016), The Cryosphere, 12, 1479–1498, 2018.